Structural Engineering and Mechanics, Vol. 4, No. 3 (1996) 257-276
DOI: http://dx.doi.org/10.12989/sem.1996.4.3.257

Numerical simulation of concrete slab-on-steel girder bridges with frictional contact

Jian Jun Lin†

Forintek Canada Corporation, National Wood Products Research Institute, Canada

Mario Fafard‡ and Denis Beaulieu‡†

Department of Civil Engineering, Laval University, Canada

Abstract. In North America, a large number of concrete old slab-on-steel girder bridges, classified noncomposite, were built without any mechanic connections. The stablizing effect due to slab/girder interface contact and friction on the steel girders was totally neglected in practice. Experimental results indicate that this effect can lead to a significant underestimation of the load-carrying capacity of these bridges.

In this paper, the two major components-concrete slab and steel girders, are treat as two deformable bodies in contact. A finite element procedure with considering the effect of friction and contact for the analysis of concrete slab-on-steel girder bridges is presented. The interface friction phenomenon and finite element formulation are described using an updated configuration under large deformations to account for the influence of any possible kinematic motions on the interface boundary conditions. The constitutive model for frictional contact are considered as slip work-dependent to account for the irreversible nature of friction forces and degradation of interface shear resistance. The proposed procedure is further validated by experimental bridge models.

Key words: composite action; contact; degradation; finite element; friction.

1. Introduction

Numerous concrete slab-on-steel girder bridges were built in North America over the last few decades. These bridges, termed noncomposite bridges, are characterized by the fact that the concrete slab simply rests on steel girders with no mechanical connection at the concrete/steel interface. In practice, it is widely accepted that the two major components do not interact and generally assumed that only the steel girders sustain loads. Evaluations of load carrying capacities, based on this design philosophy, predicts that bridges built two decades ago are far from able to sustain modern traffic loads. However, most of them are still in use and perform well under heavy traffic loads. Experimental studies showed that the discrepancy between theorical prediction and actual load carrying capacity can be attributed to the presence of fricition forces and contact

† Research Fellow
‡ Associate Professor
‡† Professor

at the concrete slab/steel girder interface (Dionne *et al.* 1991).

Frictional contact effects are of prime importance in engineering applications, such as the design of mechanical connections and rock mechanics. There exist two major approaches in previous investigations to the interface contact phenomenon. The first approach based on the adoption of theoretical principles such as the variational principle. Relatively sophisticated interface constitutive laws were then defined with consideration of the interface boundary conditions, compatibility and the properties of the interface media (Burdekin *et al.* 1978, Michalowski and Mróz 1978, Curnier 1984). The other approach consisted in using numerical approximations, generally based on the finite element method, to simulate the interface phenomenon with either classical or modified Coulomb's friction law (Fredriksson 1976, Okamoto and Nakazawa 1979, Sachedeva, and Ramakrishnan 1981, Torstenfelt 1983). These previous studies, whether theoretical or numerical, are basically focused on solid mechanics problems limited, almost entirely, to a deformable body resting on a rigid foundation (Signorini-Fichera problem) with a monotonically increasing contact area as load increases. However, this may not always be the case for a deformable body on a deformable foundation (like Winkler foundation) since the contact area can decreases as load increases. Furthermore, if both material and geometrical nonlinearities are included in the analysis of a contact problem, the variation of relative rigidities of contacting bodies and change of configurations due to large geometrical deformations certainly affect the interface boundary conditions and compatibility. Taking these factors into account, the classical approaches are obviously not suitable and a more sophisticated analysis is required.

This study focuses on the frictional contact problems between two deformable bodies. The interface displacements and contact forces are described using updated geometrical configurations in order to capture the possible variations of interface boundary conditions induced by large deformations and rigid body motions. Interface constitutive laws are established by assuming independence between the normal and tangential directions. A model for the interface shear resistance, inspired by a number of published models, is proposed with considering interface slip rate and shear resistance degradation. The model modifies the classical isotropic Coulomb's law used to define the onset of interface slip. In the finite element approach to the contact problem, it is assumed that two deformable bodies in contact are subject to the given boundary conditions. Special considerations are also given to the post-separation and post-slip interface phenomena which are discussed in a context of numerical analysis. Finally, two numerical examples are presented for the validation of the proposed interface model and numerical procedures. The numerical results closely resemble the experimental ones.

2. Frictional contact under large deformations

Slab-on-steel girder bridges are essentially composed of thin concrete slabs and steel plates. When subjected to heavy loading, these two major components may undergo large deformations, and the concrete slab behaves like a plate on a deformable foundation, especially as no mechanical connection is provided at the interface. Unlike the classical contact problem, in which the contact surface increases monotonically under different load levels, the contact area at the interface in our problem can either increase or decrease, varying with the geometrical configuration and material state of two deformable bodies in contact. Therefore, an appropriate description of variation of contact surface and frictional features between two deformable bodies requires proper

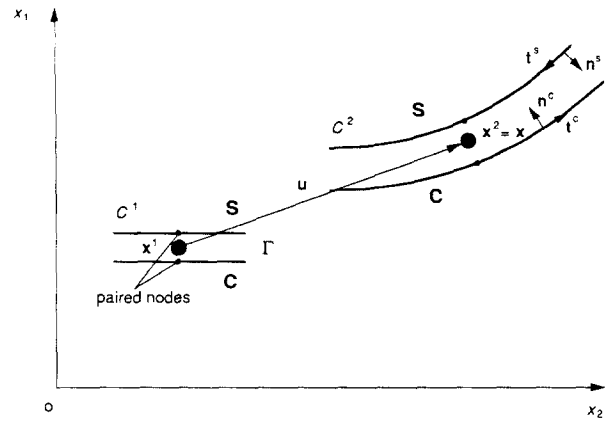

Fig. 1 Interface relative displacements under large deformations.

definitions of relative displacements and frictional contact forces at the interface. The following description assumes large geometrical deformations and small interface displacements.

Fig. 1 shows two deformable bodies C and S in contact. The coordinate and displacement vectors are ${}^{c(s)}\underset{\sim}{x}^{\alpha}$ and ${}^{c(s)}\underset{\sim}{u}^{\alpha}$, respectively, and ${}^{c(s)}\underset{\sim}{n}^{\alpha}$ is the outward normal boundary vector with n_i oriented in the direction of the corresponding coordinate axes x_i. The right superscript α $(=1, 2)$ refers to configurations C^1 and C^2 of the deformable bodies. Configuration C^1 is considered as a previous loading step in equilibrium. To make description easier, the increments of relative displacements for the establishment of constitutive relationships and the total relative displacements for the definition of the interface contact conditions under current configuration C^2 in two dimensional space (either x-y or n-t plane) are defined. These descriptions can be extrapolated to three dimensional space by considering that $\underset{\sim}{t}$ has two components, t_1 and t_2 in the tangential plane. Note that we use ${}^{\beta}x_i$ for ${}^{\beta}x_i^2$ and ${}^{\beta}n_i$ for ${}^{\beta}n_i^2$ (*i, summation convention*) in the following descriptions.

2.1 Relative interface displacements

The increment of normal relative displacement at the interface between two configurations can be expressed as:

$$\Delta d_n = d_n - d_n^1. \tag{1}$$

The total normal relative displacement is

$$d_n = -({}^{c}n_i\,{}^{c}x_i + {}^{s}n_i\,{}^{s}x_i), \tag{2}$$

with ${}^{\beta}n_i$ defined on configuration C^2 and

$${}^{\beta}x_i = {}^{\beta}x_i^1 + {}^{\beta}u_i \quad \beta = c,\ s, \tag{3}$$

where ${}^{\beta}u_i$ represents the incremental displacements between two configurations.

Similarly, the increment of relative tangential displacement can be defined as

$$\Delta\underset{\sim}{d}_t = \underset{\sim}{d}_t - \underset{\sim}{d}_t^1. \tag{4}$$

The total relative tangential displacement is:

$$\underset{\sim}{d}_t = {}^c\underset{\sim}{x}_t - {}^s\underset{\sim}{x}_t \tag{5}$$

with components of ${}^\beta\underset{\sim}{x}_t$ in the direction of axes x_i given by:

$${}^\beta x_{ti} = {}^\beta\underset{\sim}{x}_t \, {}^\beta\underset{\sim}{t} = {}^\beta x_i - {}^\beta n_i \, {}^\beta n_j \, {}^\beta x_j, \quad \beta = c, \ s. \tag{6}$$

We further define the normal and tangential contact stresses as

$$\begin{aligned} \sigma_n &= {}^c\sigma_{ij} \, {}^c n_i \, {}^c n_j = {}^s\sigma_{ij} \, {}^s n_i \, {}^s n_j \\ \underset{\sim}{\sigma}_t &= {}^c\underset{\sim}{\sigma}_t = -{}^s\underset{\sim}{\sigma}_t, \end{aligned} \tag{7}$$

where ${}^\beta\sigma_{ti} = {}^\beta\sigma_{ij} \, {}^\beta n_j - \sigma_n \, {}^\beta n_i$ and σ_{ij} is the interface stress tensor at configuration C^2.

2.2 Interface boundary conditions

Interface constraint variations, such as contact-separation and sticking-sliding phenomena, cause structural nonlinearity and rigid motion. For a candidate point at interface Γ, the possible changes of boundary condition may be either one of the following:

$$\begin{array}{cc} \textit{At configuration } C^1 & \textit{At configuration } C^2 \\ \begin{cases} \text{separation} & d_n^1 > 0 \\ \text{contact} & d_n^1 \le 0 \end{cases} \Rightarrow & \begin{cases} \text{separation} & d_n^1 + \Delta d_n \ge 0 \\ \text{contact} & d_n^1 + \Delta d_n < 0 \end{cases} \end{array} \tag{8}$$

where $\underset{\sim}{\sigma} = \{\sigma_n, \ \underset{\sim}{\sigma}_t^T\}^T$. The case $d_n < 0$ indicates that relative normal deformation is allowed in the normal direction if the deformation of interface asperities is considered. The case $d_n = 0$ with $\sigma_n = 0$ implies the existence of a special neutral condition between contact and separation. In the proposed model, the neutral condition is associated to separation since it is later assumed as in contact that d_n can be less than zero due to the adoption of the penalty method.

Interface separation means the loss of interface rigidities and the elimination of contact forces and as well as the introduction of plastic displacement flows in the tangential and normal directions. On the other hand, when bodies are in contact at the interface, either sticking or slipping occurs in the tangential direction and can be justified by:

$$\begin{aligned} &\text{if } \|\underset{\sim}{\sigma}_t\| \le \bar{\sigma}_t, \text{ sticking: } \|\Delta\underset{\sim}{d}_t^p\| = 0, \\ &\text{if } \|\underset{\sim}{\sigma}_t\| \ge \bar{\sigma}_t, \text{ slipping: } \|\Delta\underset{\sim}{d}_t^p\| \ne 0, \end{aligned} \tag{9}$$

where $\bar{\sigma}_t$ is the limit of interface shear resistance. The determination of the onset of slipping requires the introduction of a proper yield function F, and the determination of its magnitude and direction requires the selection of an appropriate plastic displacement potential Φ whose gradient defines the plastic displacement:

$$\Delta\underset{\sim}{d}^p = d\lambda \frac{\partial \Phi}{\partial \underset{\sim}{\sigma}}. \tag{10}$$

In this equation $d\lambda > 0$ is a scalar. The selection of these two functions will be discussed in the following section.

3. Interface constitutive approach

In the constitutive modeling of interface contact features, proper relationships need to be established between the interface stresses (forces) and displacements, as well as the criterion to account for the variations of the interface boundary conditions. In order to establish these constitutive relationships, the following assumptions are made:

(i) The interface media can be treated as orthotropic material in the normal and tangential directions and the constitutive relationships are assumed independent in the normal and tangential directions.

(ii) When a pair of nodes is in contact at the interface, the behavior remains elastic in the normal direction. Separation at the interface is analogous to concrete crushing which means that rigidity and internal forces vanish in both directions.

(iii) The change of state (contact or separation) of the interface only depends on the contact force or relative displacement in the normal direction. It does not depend on the state of sticking or sliding in the tangential direction under current configuration.

(iv) Material properties are assumed isotropic in the tangential plane of the interface. The interface frictional forces are only associated with the corresponding relative displacements of the two contact nodes.

The incremental constitutive relationship of an interface can be written in the form of the well-known Hooke's law

$$\Delta\sigma_k = h^e_{kl}\Delta d_l \quad i,\ l=n,\ t, \tag{11}$$

where h^e_{kl} is the elastic interface stiffness matrix.

However, Hooke's law only holds for the elastic portion. Since the analysis is nonlinear, elasto-plasticity has to be used as framework for the constitutive law. The interface relative deformation in Eq. (11) is therefore decomposed into a recoverable elastic component and a nonrecoverable plastic component in the following incremental form:

$$\Delta\underset{\sim}{d} = \Delta\underset{\sim}{d}^e + \Delta\underset{\sim}{d}^p, \tag{12}$$

It is noted that $\Delta\underset{\sim}{d} = \{\Delta d_n\ \Delta\underset{\sim}{d}_t^T\}^T$. The incremental elasto-plastic constitutive relationship can be formulated in a general form (Zienkiewicz 1977):

$$\Delta\sigma_k = \left(h^e_{kl} - \frac{1}{\bar{h}} h^e_{kj}\frac{\partial\Phi}{\partial\sigma_j}\frac{\partial F}{\partial\sigma_m}h^e_{ml}\right)\Delta d_l \tag{13}$$

where scalar $\bar{h}$ is given by (Yamaguchi and Chen 1990):

$$\bar{h} = \frac{\partial F}{\partial\sigma_m}h^e_{mj}\frac{\partial\Phi}{\partial\sigma_j} + \frac{h^p}{\sigma_{eq}}\frac{\partial F}{\partial\sigma_{eq}}\frac{\partial\Phi}{\partial\sigma_k}\sigma_k. \tag{14}$$

in which σ_{eq} is the effective contact stress and h^p is the plastic modulus.

From assumption (i) and (ii), h_{kl} is zero if $k \neq l$. Also, the constitutive relationships and yield conditions can be defined separately for the normal and tangential directions.

3.1 Normal direction

The interface separation and contact are normally defined in many publications by the use

of the interface total displacement d_n. However, the situation may be ambiguous if the nonpenetration condition is imposed in the normal direction, since $d_n=0$ may indicate that the interface is in a state of either contact or separation. By examing Eq. (8), it is found that the normal contact force may be more suitable to characterize the boundary conditions in the normal direction. In this study, the criterion describing the condition in the normal direction is:

$$F_n(\sigma_n)=\sigma_n \tag{15}$$

If a finite negative normal relative displacement is allowed to represent the normal deformation of the interface asperities, Eq. (15) can also be expressed as a function of the normal deformation d_n. The interface contact conditions can be described as:

$$\begin{cases} F_n<0 \ (d_n\leq 0) & \|\underset{\sim}{\sigma}\|\geq 0, \\ & \Rightarrow \\ \text{contact} & h_n=h_n^e \\ F_n=0 \ (d_n>0) & \|\underset{\sim}{\sigma}\|=0, \\ & \Rightarrow \\ \text{separation} & h_n=h_t=0 \end{cases} \tag{16}$$

In the above equations, Assumption (iii) is considered. As the deformable bodies are in contact at the interface, the normal displacement $d_n<0$, if allowed, only contains the elastic component. On the other hand, the separation of the deformable bodies at the interface causes the loss of both normal and tangential rigidities and the vanishing of the corresponding contact forces. If the normal plastic displacement potential function Φ_n is set identical to F_n (associated flow rule) for the state of separation, the incremental normal plastic displacement can be written unilaterally on the basis of Assumption (ii) as:

$$\Delta d_n^p=d\lambda_n\left(\frac{\partial \Phi}{\partial \sigma_n}\right)=d\lambda_n\left(\frac{\partial F_n}{\partial \sigma_n}\right)=d\lambda_n. \tag{17}$$

In this equation, $d\lambda$ is physically associated to the incremental normal displacement but no explicit expression exists since separation indicates the loss of interface rigidities and rigid body motions between paired nodes. However, for a system previously in equilibrium, a definite value for $d\lambda$ exists if the loss of partial interface rigidities does not affect the achievement of a new equilibrium state and if the released forces can be dissipated. The $d\lambda$ value generally depends on the history of the interface stress state and boundary conditions.

3.2. Tangential direction

Deformable bodies in contact can stick to each other or slide under loading. The situation depends on the current interface stress (or contact force) state and the current interface shear resistance $\bar{\sigma}_t>0$. If the classical isotropic Coulomb's law is used, the shear resistance can be expressed as:

$$\bar{\sigma}_{t\max}=\mu_0|\sigma_n|. \tag{18}$$

where μ_0 is a constant friction coefficient. This law is restricted to elastic contact problems with finite slip (Curnier, 1984). However, experimental results showed that the coefficient of friction

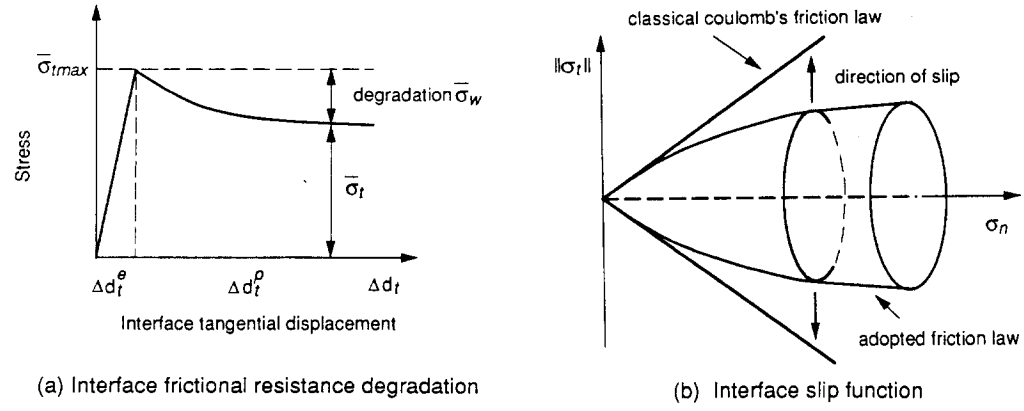

(a) Interface frictional resistance degradation (b) Interface slip function

Fig. 2 Interface friction law.

decreases with increasing relative displacements between rough concrete and steel surfaces in contact (Rabbat and Russel 1988, Labonte *et al.* 1991) A similar phenomenon has been observed at the interface between different other materials (Plesha and Belytschko 1985). Several researchers showed that the variation can be attributed to the deformable asperities, the sliding velocity, or the interface stress history. Two approaches have been proposed to simulate the interface frictional mechanism. In the first approaches, the interface shear resistance is assumed proportional to a weighted measure of the normal stresses in the vicinity of the candidate point (Burdekin *et al.* 1978, Michalowski and Mróz 1978). In the second, the shear resistance is either associated with the normal deformation of interface asperities or with the sliding velocity (Fredriksson 1976, Plesha and Belytschko 1985). A few realistic friction laws, analogous to general granular material stress-strain diagram are depicted in the literature (Panagiotopoulos 1985, Klarbring 1985) and have qualitatively described the relationship existing between interface friction force and tangential slip.

Based on experimental results and the Curnier's study (1984), the interface shear resistance may explicitly be expressed as:

$$\bar{\sigma}_t = \bar{\sigma}_{t\max} - \bar{\sigma}_w, \tag{19}$$

in which $\bar{\sigma}_{t\max}$ can be obtained using classical Coulomb's law given by Eq. (18). The condition that $\bar{\sigma}_w > 0$ recognizes irreversible degradation of the interface shear resistance, and is a funtion of the previous contact stress history and slip velocity. In this study, it is simply assumed that $\bar{\sigma}_w$ is given by:

$$\bar{\sigma}_w = \bar{\sigma}_{t\max} - \mu|\sigma_n|, \tag{20}$$

where:

$$\mu = \mu_0 exp\left\{-\omega \|\Delta \underset{\sim}{d}_t^p\| \frac{\|\underset{\sim}{\sigma}_t\|}{|\sigma_n|}\right\}$$

Parameter ω is the degradation constant and has units *force/* (*length*·*force*). It reflects properties of contact surface for the given materials of two contact bodies. The plastic tangential work $W_t^p = \|\Delta \underset{\sim}{d}_t^p\| \cdot \|\underset{\sim}{\sigma}_t\|$ in Eq. (20) is the plastic tangential work W_t^p and implies that interface degrada-

tion can occur with either high tangential force or large slip velocity (Plesha and Belytschko 1985). The term σ_n in the previous expression moderately reflect its effect on the interface shear resistance due to the change of contact area at a candidate point or region, as the normal contact stress varies (Burdekin *et al.* 1978)

The value of $\|\underset{\sim}{\sigma}_t\|/|\sigma_n|$ can be taken as the effective value of μ at previous configuration C^1. When the structure is loaded statically, this value gradually decreases with the increase of slip. This also matches the experimental observation that the deterioration of the interface shear resistance is accompanied by gradual slip increase, as shown in Fig. 2a.

It is now possible to construct the yield function to define the onset of interface slip. The classical form of the isotropic Coulomb's law is used with interface degradation considered by using assumption (iv):

$$\begin{aligned} F_t &= \|\underset{\sim}{\sigma}_t\| - \bar{\sigma}_t \\ &= \|\underset{\sim}{\sigma}_t\| - \mu|\sigma_n|, \end{aligned} \tag{21}$$

where μ is defined by Eq. (20) and represents the degenerated coefficient. The stick-sliding condition is then explicitly defined as:

$$\begin{cases} F_t<0 \Rightarrow \text{sticking} & d\underset{\sim}{\varepsilon}_t^p=0, \\ F_t=0 \Rightarrow \text{sliding} & \exists \lambda_t\, d\underset{\sim}{\varepsilon}_t^p=d\lambda_t \dfrac{\partial \Phi}{\partial \underset{\sim}{\sigma}_t},\ h_t=0. \end{cases} \tag{22}$$

The yield function $F_t=0$ defines the slip surface, as shown in Fig. 2b. It can be seen that the interface shear resistance deterioration is no longer linear with the increase of normal pressure.

It the tangential plane, σ_t can be treated as the effective stress and is expressed as:

$$\sigma_t=\|\underset{\sim}{\sigma}_t\|=\sqrt{\sigma_{t1}^2+\sigma_{t2}^2}. \tag{23}$$

A function identical to F_t for the plastic displacement potential function Φ_t. Its derivative can be easily expressed as:

$$\frac{\partial \Phi_t}{\partial \sigma_{ti}}=\frac{\partial F_t}{\partial \sigma_{ti}}=\frac{\partial \Phi_t}{\partial \sigma_t}\frac{\partial \sigma_t}{\partial \sigma_{ti}}+\frac{\partial \Phi_t}{\partial \mu}\frac{\partial \mu}{\partial \sigma_{ti}}. \tag{24}$$

The interface slip increment is obtained by substituting Eq. (19) into Eq. (24), then into Eq. (21).

$$d\varepsilon_{ti}^p=d\lambda\frac{\partial \Phi_t}{\partial \sigma_{ti}}=d\lambda'\frac{\sigma_{ti}}{\sqrt{\sigma_{t1}^2+\sigma_{t2}^2}}\,\text{sign}(\sigma_{ti}) \quad i=1,\ 2 \text{ (no sum on } i), \tag{25}$$

with

$$d\lambda'=d\lambda(1+\mu\omega\|\Delta\underset{\sim}{d}_t^p\|)>d\lambda>0.$$

Parameter $d\lambda$ in Eq. (25) indicates that the interface slip components are proportional to the interface frictional forces and $\mu\omega\|\Delta\underset{\sim}{d}_t^p\|$ is the rate of slip caused by the interface shear deterioration.

4. Finite element approach

In the finite element modeling of frictional contact, the interface media Γ between two subdomains C and S is discretized by sets of paired nodes along the span, as shown in Fig. 1. The notation C and S denote concrete and steel, respectively. The properties of the contact elements, which link paired nodes with linear interpolation, are assumed to properly characterize the interface media. The vector $\{\Delta d_n, \underset{\sim}{\Delta d}_t^T\}^T$, defined in Eqs. (1) and (4) represents the set of updated relative displacement increments of a considered pair of nodes. The contact stresses are transferred by finite element approximation to the set of equivalent nodal forces with its components $\{f_n, \underset{\sim}{f}_t^T\}$ expressed in the local coordinate system. Correspondingly, the moduli h^e and h^p in Eq. (13) are replaced by k and k^p.

4.1. Updated Lagrangian formulation

The finite element approximation of the entire system can be obtained from the variational principle (Lin *et al.* 1991, Fafard *et al.* 1993). It can be written in an incremental updated formulation as:

$$W = W_2^2 + (\Delta W)_2 = 0, \tag{26}$$

where W_2^2 defines the contribution of residual forces in the estimated configuration C^2 (superscript) using the C^2 geometrical space descriptions (subscript), and $(\Delta W)_2$ is the improvement required to achieve system equilibrium at step $C(t)$-C^2. The discretized form of Eq. (26) is expressed as:

$$[K_T]\underset{\sim}{\Delta U} = \underset{\sim}{R}, \tag{27}$$

where $[K_T]$ is the updated tangential stiffness matrix and $\underset{\sim}{R}$ is the residual vector. If no interaction exists at the interface of subdomains S and C, Eq. (27) represents two independent groups of equations:

$$\begin{bmatrix} K_S & 0 \\ 0 & K_C \end{bmatrix} \begin{Bmatrix} \underset{\sim}{\Delta U}_S \\ \underset{\sim}{\Delta U}_C \end{Bmatrix} = \begin{Bmatrix} \underset{\sim}{R}_S \\ \underset{\sim}{R}_C \end{Bmatrix} \tag{28}$$

Eq. (28) is modified to include the contribution of the interface media by introducing equilibrium conditions at the common boundary of C and S. It is assumed that the following equilibrium condition in incremental form is satisfied at interface Γ:

$$L\ (\underset{\sim}{\gamma}) + \underset{\sim}{R}_I = 0 \tag{29}$$

where L is a simple *linear* operator since linear interpolation is adopted, and $\underset{\sim}{\gamma}$ is the vector of interface incremental displacement equivalent to $\underset{\sim}{\Delta d}$. Vector $\underset{\sim}{R}_I$ is the vector of residuals acting on interfact Γ. Another incremental variational formulation can be written for the entire system by introducing Eq. (29) into Eq. (26)

$$W = W_C + W_S + \int_\Gamma (\underset{\sim}{\lambda}^*)^T (L(\underset{\sim}{\gamma}) + \underset{\sim}{R}_I) d\Gamma \tag{30}$$

where W_C and W_S are the incremental virtual work related to C and S, respectively. The multiplier $\underset{\sim}{\lambda}^*$ is a virtual displacement vector and has to be boundary admissible. In the present case,

$\underset{\sim}{\lambda}$ is identical to the relative interface displacement vector $\underset{\sim}{\gamma}$ so that Eq. (30) can be written as:

$$\int_{\Gamma}(\underset{\sim}{\lambda}^*)^T(L(\underset{\sim}{\gamma})+\underset{\sim}{R}_I)d\Gamma=(\underset{\sim}{\gamma}^*)^T\int_{\Gamma}L(\underset{\sim}{\gamma})d\Gamma+(\underset{\sim}{\gamma}^*)^T\int_{\Gamma}\underset{\sim}{R}_I d\Gamma \tag{31}$$

where $\underset{\sim}{\gamma}=\{\Delta d_n, \underset{\sim}{\Delta d}_t^T\}^T$. A linear interpolation between the interface paired nodes is adopted and given below:

$$L(\underset{\sim}{\gamma})=[\kappa_T]([^cR]^c\underset{\sim}{u}-[^sR]^s\underset{\sim}{u}), \tag{32}$$

where $[\kappa_T]$ is the constitutive matrix for the interface in the local coordinate system. Matrices $[^cR]$ and $[^sR]$ are the transformation matrices which transfer the boundary displacement increments ${}^c\underset{\sim}{u}$ and ${}^s\underset{\sim}{u}$ respectively to the local system defined by vector $\{\underset{\sim}{n},\underset{\sim}{t}\}$. These matrices are derived from Eqs. (1) to Eq. (5). Substituting Eq. (32) into (31), the virtual work of the whole system in a discretized incremental form is obtained as:

$$\begin{aligned}W=W_C+W_S&+({}^c\underset{\sim}{u}^{*T}[^cR]^T-{}^s\underset{\sim}{u}^{*T}[^sR]^T)[\kappa_T]([^cR]^c\underset{\sim}{u}-[^sR]^s\underset{\sim}{u})\\&+({}^c\underset{\sim}{u}^{*T}[^cR]^T-{}^s\underset{\sim}{u}^{*T}[^sR]^T)\int_{\Gamma}\underset{\sim}{R}_I d\Gamma.\end{aligned} \tag{33}$$

Let $\Delta\underset{\sim}{U}_C$ and $\Delta\underset{\sim}{U}_S$ be the displacement increments of subdomains C and S. Note that ${}^c\underset{\sim}{u}\in\Delta\underset{\sim}{U}_C$ and ${}^s\underset{\sim}{u}\in\Delta\underset{\sim}{U}_S$. The third and fourth terms in Eq. (33) only modify the elements in the global stiffness matrix and the global nodal force vector associated with ${}^c\underset{\sim}{u}$ and ${}^s\underset{\sim}{u}$. The modification will not increase or decrease the number of equations of the global system (Zienkiewicz 1977).

Displacement sets $\Delta\underset{\sim}{U}_C$ and $\Delta\underset{\sim}{U}_S$ can be partitioned as $\Delta\underset{\sim}{U}_C=\{\underset{\sim}{u}_c, {}^c\underset{\sim}{u}\}^T$ and $\Delta\underset{\sim}{U}_S=\{{}^s\underset{\sim}{u}, \underset{\sim}{u}_s\}^T$ and corresponding nodal force vectors as $\underset{\sim}{R}_c=\{\underset{\sim}{r}_c, {}^c\underset{\sim}{r}\}^T$ and $\underset{\sim}{R}_S=\{{}^s\underset{\sim}{r}, \underset{\sim}{r}_s\}^T$. Invoking equibrium for the whole system in the discretized form of Eq. (33), by setting virtual work W equal to zero and recalling that $\underset{\sim}{u}_c{}^*$, ${}^c\underset{\sim}{u}^*$, ${}^s\underset{\sim}{u}^*$ and $\underset{\sim}{u}_s{}^*$ are arbitrary virtual displacement sets, the following is obtained:

$$\begin{bmatrix} K_{11} & K_{1c} & 0 & 0 \\ K_{1c} & K_{cc}+I_{cc} & -I_{sc} & 0 \\ 0 & -I_{cs} & K_{ss}+I_{ss} & K_{2s} \\ 0 & 0 & K_{2s} & K_{22} \end{bmatrix} \begin{Bmatrix} \underset{\sim}{u}_c \\ {}^c\underset{\sim}{u} \\ {}^s\underset{\sim}{u} \\ \underset{\sim}{u}_s \end{Bmatrix} = \begin{Bmatrix} \underset{\sim}{r}_c \\ {}^c\underset{\sim}{r}-[^cR]^T\underset{\sim}{R}_I \\ {}^s\underset{\sim}{r}+[^sR]^T\underset{\sim}{R}_I \\ \underset{\sim}{r}_s \end{Bmatrix} \tag{34}$$

where ${}^c\underset{\sim}{r}$ and ${}^s\underset{\sim}{r}$ are modified as ${}^c\underset{\sim}{r}-[^cR]^T\underset{\sim}{R}_I$ and ${}^s\underset{\sim}{r}+[^sR]^T\underset{\sim}{R}_I$, respectively. In Eq. (34), the term of the matrix modified by I represent the interactions at the interface between S and C. If $[\kappa_T]$ is a zero matrix, the stiffness matrix becomes to $[K_T]$ as in Eq. (28).

In this study, the contact mechanisms and mechanical connections are simulated by the use of a bar element linking to two nodes (Lin *et al.* 1991). The bar element can be treated as two independent linear springs having a siffness k_t, perpendicular to the longitudinal axis of the bar and k_n, parallel to the longitudinal axis of the bar. Bar rigidities k_n and k_t should represent the average interface behavior of the materials in contact.

For a pair of nodes currently in contact, the non-penetration condition in the normal direction is physically simulated with penalty approximation by assigning a large value to the initial rigidity k_n. From a numerical point of view, the rigidity of the contact element in the normal direction should be larger than the local rigidity of the bodies in contact. A reasonably large

value of k_t is assumed to make the interface act as a linear spring before slipping. A proper choice of values for these two parameters depends upon the type of structure analyzed and individual experiences.

4.2. Numerical considerations

As previously mentioned, contact problems often imply variations of the interface boundary conditions. In the finite element approach, these variations are not known in advance for a given load increment. An iterative procedure should ensure the verification of the physical changes and proper numerical considerations should be given to account for the post-separation and post-slip performance of the interface media. The following set of incremental formulations is evaluated iteratively on the basis of the updated configuration C^2. Any variation of contact and separation of a paired node in the normal direction is verified by:

$$\left.\begin{array}{r} f_n=f_n^1+k_n\Delta d_n\geq 0 \\ \text{or } d_n\geq 0 \end{array}\right\}\Rightarrow\text{separation, so}\quad \begin{array}{l} f_n^2=\underset{\sim}{f_t^2}=0 \\ k_n^2=k_t^2=0 \end{array}$$

$$\left.\begin{array}{r} f_n=f_n^1+k_n\Delta d_n<0 \\ \text{or } d_n<0 \end{array}\right\}\Rightarrow\text{contact, then}\quad \begin{array}{l} f_n^2=f_n<0 \\ \underset{\sim}{f_t^2}=\underset{\sim}{f_t^1}+k_t^2\Delta\underset{\sim}{d_t}\neq 0 \end{array} \tag{35}$$

in which k_n is the initial normal rigidity. The superscripts 1 and 2 refer to the terms evaluated at C^1 and C^2, respectively. The f_n and d_n values play an equivalent role in the verification of the interface boundary conditions since d_n can be a finite negative value as long as k_n is not equal to infinity. The ambiguity attributed to $d_n=0$ disappears in the finite element analysis since the direct stiffness method is used.

In the tangential direction, the discretized form of Eq. (21) is used as yield function to define the onset of interface slip:

$$F_t=\|\underset{\sim}{f_t}\|-\mu|f_n|=0, \tag{36}$$

As in Eq. (21), μ is used instead of μ_0 to reflect the interface degradation with σ_n and $\underset{\sim}{\sigma_t}$ replaced by f_n and $\underset{\sim}{f_t}$, respectively.

$$\begin{aligned} &\|\underset{\sim}{f_t}\|\leq\mu|f_n|\Rightarrow\Delta d_t^p=0 \\ &\|\underset{\sim}{f_t}\|>\mu|f_n|\Rightarrow\Delta\underset{\sim}{d_t^p}=d\lambda_t\frac{\partial F_t}{\partial\underset{\sim}{f_t}}\neq 0. \end{aligned} \tag{37}$$

It is assumed that $\underset{\sim}{f_t}$ lies in a plane defined by $\{\underset{\sim}{t_1}, \underset{\sim}{t_2}\}$ with two corresponding components, f_{t1} and f_{t2}. The following function gives a yield surface in the tangential plane:

$$F_t=\sqrt{(f_{t1})^2+(f_{t2})^2}-\mu|f_n|=0 \tag{38}$$

4.3. Post-separation and post-slip

Since interface separation and slip introduce rigid body motions which may cause singularities in the solution of a problem, special considerations are required during the interface separation

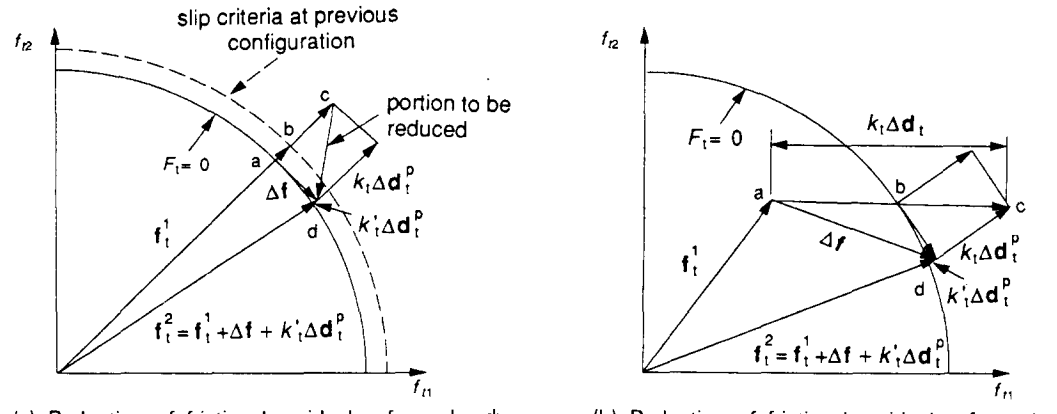

(a) Reduction of frictional residuals of an already sliped pair of nodes

(b) Reduction of frictional residuals of a pair of nodes at initial slip

Fig. 3 Reduction of frictional residuals.

and slip. This problem occurs in the analysis of a concrete slab-on-steel girder bridge when a substantial drop on contact surface area with increasing material plasticity leads to an ill-conditioned stiffness matrix $[K_T]$. Moreover, separation and slip indicate the release of interface contact forces. The redistribution of these forces requires the knowledge of the contact history and the use of a proper solution technique of iterative nature.

For a candidate pair of nodes in contact at a given load step and separated at the following step, loss of rigidity and free motions in both normal and tangential directions occur. Physically, rigidities should be set to zero to satisfy the compatibility of displacements at the interface. However, this often leads to numerical difficulties and, as a result, the solution diverges. The stiffness matrix may be seriously ill-conditioned as more paired nodes lose contact. To avoid these potential numerical problems, it is preferable to use very small fictive values k'_l ($l=n, t$) instead of zero for the interface rigidities.

The excess tangential force $\|\underset{\sim}{f}_t\| - \mu|f_n|$ must be eliminated by bringing the estimated tangential forces back to the yielding surface defined by F_t. Since the $\|\underset{\sim}{f}_t\|$ value is initially calculated by assuming elastic behavior for the incremental displacement $\underset{\sim}{\Delta d}_t$, the portion of tangential force which needs to be reduced is:

$$\|\Delta \underset{\sim}{r}_t\| = k_t \|\Delta \underset{\sim}{d}_t^p\| = \|\underset{\sim}{f}_t\| - \mu|f_n| \tag{39}$$

For a pair of nodes previously in contact, the reduction procedure for the nodal force residues requires to consider two cases, as for a general elasto-plastic continuum. The first is the reduction of shear resistance due to degradation or deloading of the normal contact force which occurs in the current load step, $\overline{ab}$, as shown in Fig. 3a. In this case, the out-of-balance forces, $\|\Delta \underset{\sim}{r}_t\|$ in Eq. (39), include the portion $\overline{ab}$ due to the variation of the yielding value between two configurations and the portion $\overline{bc}$ ($k_t \underset{\sim}{d}_t^p$) with $\underset{\sim}{d}_t^p$ paralled to the tangential force. In the second case, the slip only occurs at the current load increment (initial yielding), as illustrated in Fig. 3b. The elastic behavior assumption would define the final nodal force by point c. However, according to the yield criteria, the nodal force point cannot pass the yield surface and the portion between points b and c has to be reduced. The reduction procedure has to satisfy both the normality rule and the yield condition defined by Eqs. (25) and (38). Any elastic nodal force

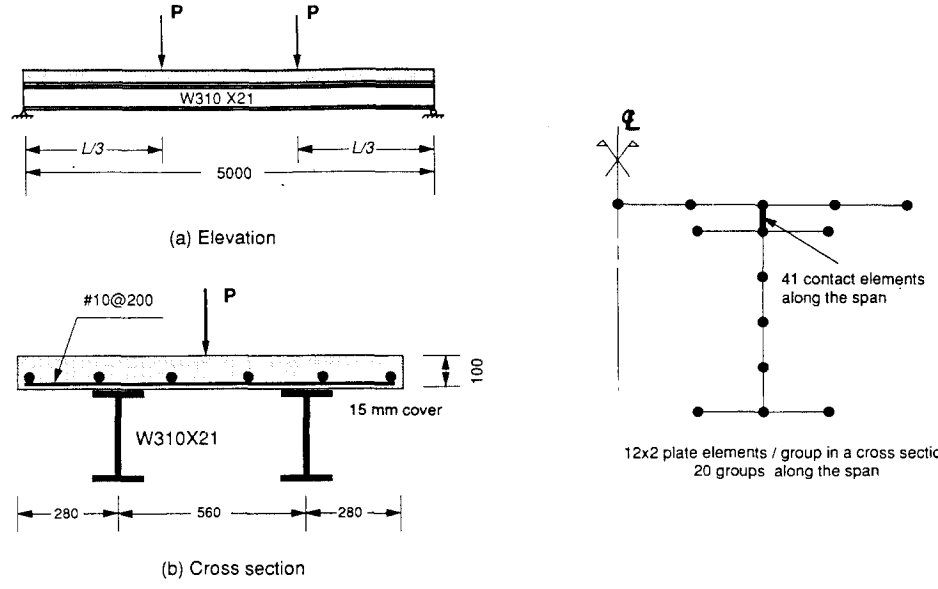

Fig. 4 Frictional contact bridge model.

increment has to move on a surface tangential to the yield surface or inside the area determined by $F_t<0$ to satisfy the yield condition. After a number of iterations for which both equilibrium and interface displacement compatibility are satisfied, the tangential force may reach a point on yielding surface, such as point d. Note that slip hardening has been considered in plotting Figs. 3a and 3b.

The residual of tangential force components for distribution, Δr_{t_i}, is written on the basis of the normality rule and Assumption (iii) as:

$$\frac{\Delta r_{t1}}{\Delta r_{t2}}=\frac{\Delta d_{t1}}{\Delta d_{t2}} \tag{40}$$

5. Numerical examples

To evaluated the importance of frictional contact, the finite element method based on the proposed model is used to simulate the behavior of some of slab-on-steel girder bridge specimens tested at Laval University (Dionne *et al.* 1991). Two numerical simulations are briefly reviewed in the present paper. The concrete slab and steel girders are discretized by using six node triangle plate/shell elements, called DLTP (Dhatt *et al.* 1986). Detailed description of the formulation of this element and constitutive relationships for concrete and steel can be found elsewhere (Lin *et al.* 1991). Properties E_c and ε_{cu}, based f_c', are calculated according to the equations proposed by ACI Committee **363** (1984) and are identified by '*'. The tensile strength f_t', also based on f_c', is calculated from the relationship proposed by Collins and Mitchell (1987) and is identified by '**'. The initial rigidities for the contact elements are set to 1×10^8 for k_n 1×10^6 for k_t. The coefficients for post-separation and post-slip are 10^{-6} for c_n and 10^{-4} for c_t. Based on Rabbat and Russel's (1988) test results, the initial Coulomb's coefficient μ_0 used is 0.5, The degradation

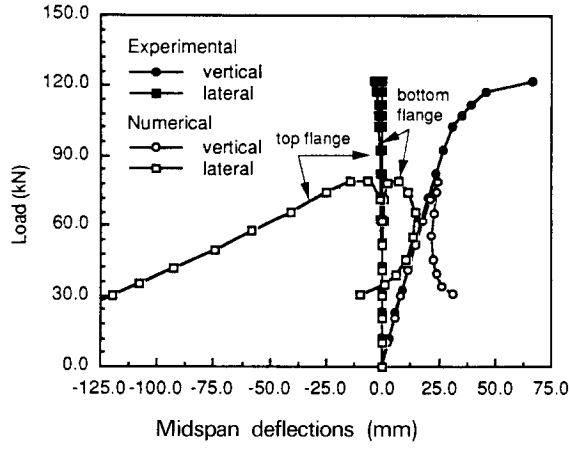

(a) Load *vs* midspan deflections ($\mu_0=0$)

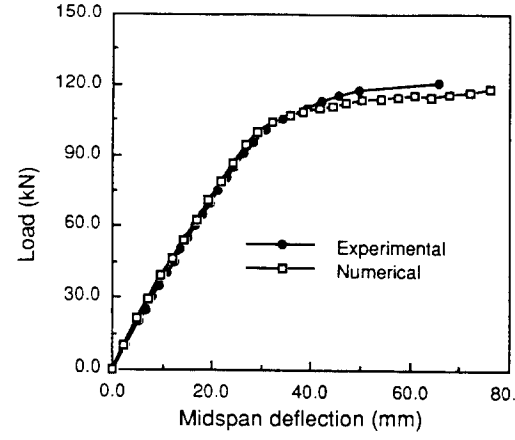

(b) Load *vs* midspan deflections ($\mu_0=0.5$)

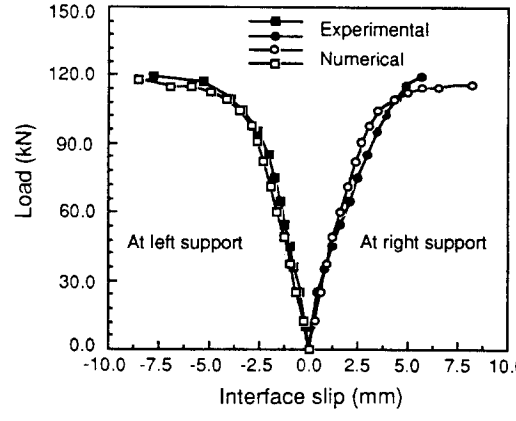

(c) Load *vs* interface slip at supports ($\mu_0=0.5$)

Fig. 5 Experimental and numerical load displacement curves of Model I.

coefficient ω in Eq. (20) depends on the properties of the interface media and is practically unknown. In the present study, we use $\omega=0.1$ obtained from trial tests.

5.1. Bridge specimen with frictional contact only (Model I)

Three identical slab-on-steel girder bridge specimens were tested to examine the beam stabilizing effect and the degree of composite action developed by interface friction. The model comprised a concrete slab of 5000×1120×100 mm concrete slab and two I-section steel beams, as shown in Fig. 4. The concrete slab was cast directly on the steel girders. No mechanical connections were provided at the interface. The loads were located at third points in the longitudinal direction and at the center of the slab in the transverse direction. The material properties are given below:

Steel		Conrete	
$f_y=350$	MPa (beam)	$f'_c=35$	MPa
$=400$	MPa (steel bar)	$f'_t=3$	MPa**

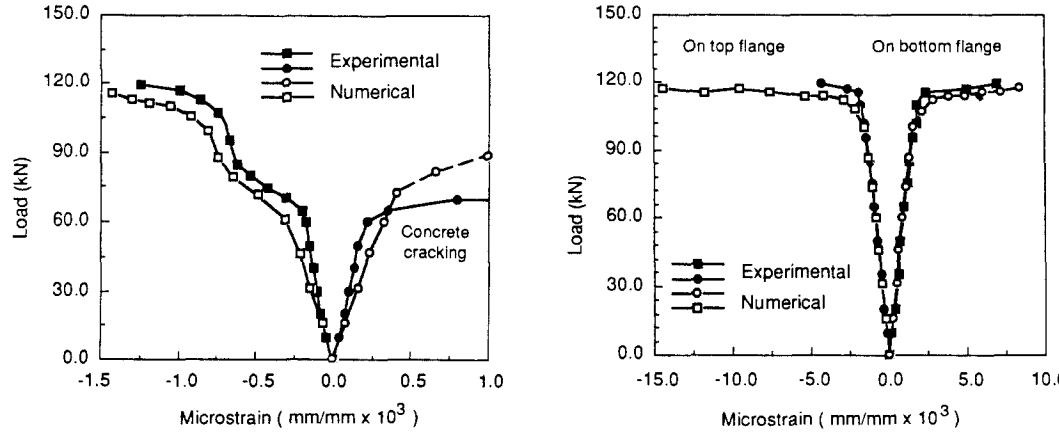

(a) Load *vs* concrete microstrain (b) Load *vs* steel microstrain

Fig. 6 Experimental and numerical load-longitudinal microstrains at midspan of Model I.

$E_s=2\times10^5$	MPa	$E_c=3\times10^4$	MPa*
$\bar{h}=0.005$	(hardening factor)	$\varepsilon_{cu}=0.0027$*	
		$\nu_0=0.2$	(assumed)

The experimental results show that these models give rather close loading responses (Dionne *et al.* 1991). The first specimen was selected for analysis and discussion since its test results represent the average responses of the tree specimens. The specimen failed at $P_u=122$ kN, as shown in Fig. 5. Yielding of the steel beam was observed at the final loading stage before the top flange of one of the steel beams buckled laterally. One half of the bridge model was analyzed. The finite element discretization of the cross section is shown in Fig. 4c. Forty one contact elements were used at the interface along the span.

The specimen was first analyzed numerically without considering the interface shear resistance ($\mu_0=0$). The model failed at 82 kN, which is 2/3 of the experimental ultimate load, while both material structural responses were still in the elastic range. The failure was caused by buckling of the beam top flange. This is confirmed by the large lateral displacements at the final loading stage and the shape of the midspan load-deflection curves against the experimental results in Fig. 5a. The model was further analyzed by taking into account the effect of interface friction with $\mu_0=0.5$. Fig. 5b presents the load *vs* midspan deflection curve obtained numerically and the corresponding experimental curve. It is observed from Figs. 5a and 5b that the initial loading responses are almost similar up to about 2/3 of the ultimate load for $\mu_0=0.0$ and 0.5. However, the curve for $\mu_0=0.0$ diverges from the experimental result at about 80 kN while the curve for $\mu_0=0.5$ follows the experimental result up to 117 kN, which corresponds to 97% of the ultimate experimental load. These results indicate that interface friction considered in the analysis does not contribute significantly to the composite action in the early loading stages because the interface separation occurs as soon as the bridge is loaded. As loading increases, large interface portions lose contact and interface friction disappears quickly. However, although the interface friction is small, it still plays an important role in stablizing the steel girder. Much larger girder capacity is achieved by using $\mu_0=0.5$.

Some numerical and experimental results are compared in Figs. 5c, 6a, and 6b. Fig. 5c shows

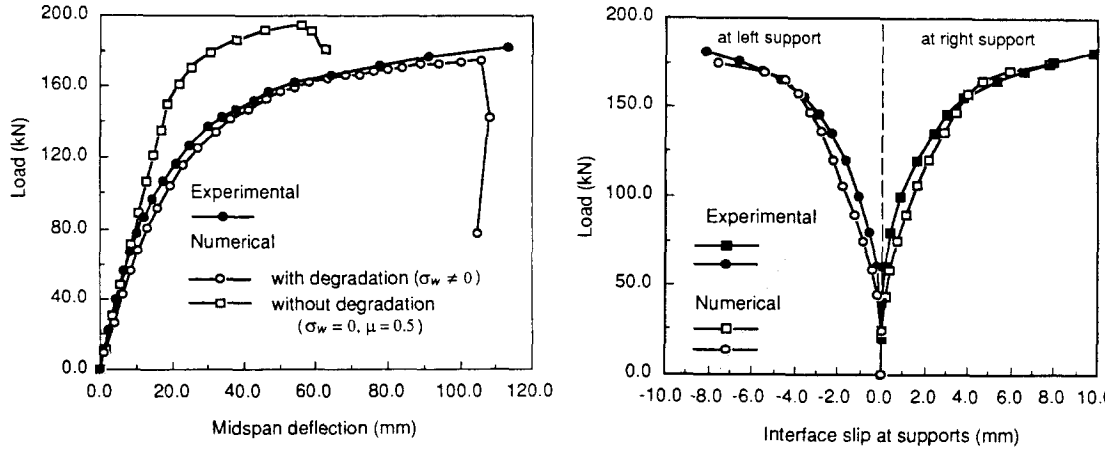

Fig. 7 Experimental and numerical load displacement curves of Model II.

load *vs* interface slip curves at two supports for model I. Figs. 5a and 5b illustrate the average concrete strain measured and calculated on the top and bottom surfaces of the slab and the longitudinal steel strain measured and calculated on the top and bottom flanges at midspan. A good agreement between the numerical and test results is oberved.

5.2 Bridge specimen with frictional contact enforced by prestressing (Model II)

Specimens were tested with the same characteristics as in the previous example except for the interface which was reinforced by 20 prestressed high strength rods. The rods connected the concrete slab to the top flange of the steel girders through drilled oversize holes. The stress in the rods was set at 400 MPa. The objective of this study was to investigate the beneficial effect of friction provided by prestressed rods on the overall specimen behavior. The experimental ultimate load P_u obtained was 182 kN. The failure was initiated by yielding of the steel girders.

The finite element idealization is as shown in Fig. 4c. The rods are simulated by bar elements with the assumption that they do not carry any interface shear. Shear forces are solely resisted by interface friction resistance. Considering the significant loss of prestress due to relaxation and creep for short bars (Collin and Mitchell 1987), the effective prestress for analysis is taken as 280 MPa (70% of the initial value). Furthermore, only prestress is applied at the first loading step to represents the real case for which prestress is applied before the model is loaded.

The failure load obtained numerically is 173 kN, which is 5% lower than the experimental value. For comparison, the bridge model is analyzed by considering the classical Coulomb's law and the proposed slip function given by Eq. (19). The resulting load *vs* midspan deflection curves are depicted in Fig. 7a. It can be seen that the load capacity is overestimated if the classical Coulomb's law is adopted. On the other hand, the model closely simulated the experimental results when the proposed slip function is used. Numerical and experimental results are compared in Figs. 7b and 8. Curves for load *vs* interface slip at supports are plotted in Fig. 7b, while load *vs* concrete and steel microstrain curves are compared in Figs. 8a and 8b, respectively. Strains were measured and calculated at midspan on the upper and lower fibres of both

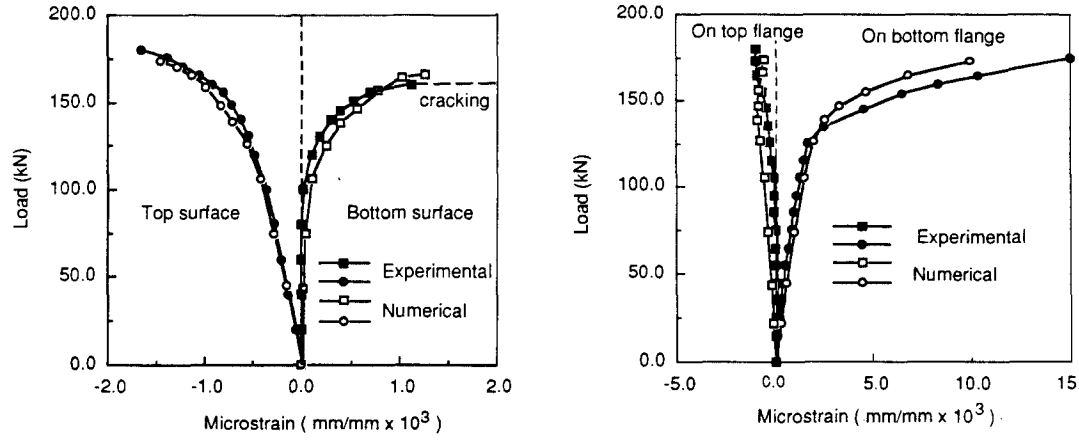

Fig. 8 Experimental and numerical load-longitudinal microstrains at midspan of Model II.

the concrete slab and the steel girders. These results, once again, prove the validity of the proposed model.

6. Concluding remarks

In this paper, the contact problem between two deformable bodies has been described in the updated geometrical configuration to account for the effects of possible large deformations and kinematic motions on the interface boundary conditions and compatibility. The interface constitutive models are assumed to act independently in the normal and tangential directions. The new interface constitutive models are established considering previous analytical, numerical and experimental investigations and include the effects of the degradation of interface shear resistance. The finite element model is formulated on the basis of an incremental updated Lagrangian procedure with consideration of interface compatibility and possible variation of interface boundary conditions by invoking the variational principle.

The proposed interface constitutive models and the finite element procedure deformable bodies in contact have proved to be very efficient in the simulation of concrete-slab-on-steel-girder bridges with frictional contact. It is shown that ignoring the influence of interface friction leads to an underestimation of the ultimate resistance of slab-on-girder bridges. On the other hand, the use of the classical Coulomb's friction law without considering the degradation of the interface shear resistance, such as the slip function, may lead to an overestimation of the ultimate load capacity of these bridges.

The proposed finite element procedure which incorporates a new interface friction law can therefore be readily used to study the load performance of slab-on-girder bridges with frictional contact. Future studies will focus on the influence of certain other factors such as materials, geometrical configurations, load types and positions, relative rigidities of the components in contact, etc. These studies will ultimately result in a series of practical recommendations for a more

realistic evaluation of the behaviour of slab-on-girder bridges and for the strengthening of these bridges.

Acknowledgements

The authors wish to thank the Quebec Ministry of Transportation, the Natural Science and Engineering Research Council of Canada and "le Fonds FCAR" for funding this project and Laval University for providing the computer facilities for the numerical analyses.

References

ACI Committee 363 (1984). "State of the art report on high strength concrete", *Amer. Conc. Inst. J.* **81** (4), 361-411.

Burdekin, M., Cowley, A. and Back, N. (1978). "An elastic mechanism for the microsliding characteristics between contacting machined surfaces", *J. Mech. Engrg. Sci.* **20** (3), 341-350.

Collins, M. P. and Mitchell, D. (1987). *Prestressed Concrete Basics*, Can. Prestressed Conc. Inst., Ottawa, Canada.

Curnier, A. (1984). "A theory of friction", *Int. J. Solids Struct.*, **20** (7), 637-647.

Dionne, G., Picard, A., Beaulieu, D. et Fafard, M. (1991), "Comportement expérimental des ponts acier-béton avec dalle de béton non-participante", Rapport, Dép. de Génie Civil, Université Laval, 293.

Dhatt, G., Marcotte, L. and Matte, Y. (1986), "A new triangular discrete Kirchhoff plate shell element", *Int. J. Num. Meth. Engrg.* **23**, 453-470.

Fafard, M., Lin, J. Massicotte, B. and Beaulieu, D. (1993). "Application of FEM for the analysis and strengthening of bridges made of concrete slabs and steel beams", *European Jour. of Finite Elements* **2** (3), 319-355.

Fredriksson, B. (1976). "Finite element solution of surface nonlinearities in structural mechanics with special emphasis on contact and fracture mechanics problems", *Comput. Struct.* **6**, 281-290.

Klarbring, A. (1985). "The influence of slip hardening and interface compliance on contact stress distributions—A mathematical programming approach", *Studies in Appl. Mech.-Mech. of Mat. Interfaces*, Series 11, Ed. A.P.S Selvadurai and G.Z. Boyiadjis, 43-59.

Labonte, J., Beaulieu, D. et Picard, A. (1991), "Étude expérimentale du coefficient de friction entre béton et acier", Rapport GCT-91-02, Dép. de Génie Civil, Université Laval, 116.

Lin, J.J., Fafard, M., Beaulieu, D. and Massicotte, B. (1991), "Nonlinear analysis of composite bridges by the finite element method", *Comput. Struct.* **40** (5), 1151-1167.

Massicotte, B., Elwi, A. E. and MacGregor, J. G. (1990). "Tension-stiffening model for planar reinforced concrete members", *J. Struct. Engrg., ASCE*, **116** (9), 3039-3058.

Michalowski, R. and Mróz, X. (1978). "Associated and non-associated sliding rules in contact friction problems", *Arch. Mech.* **30** (3), 259-276.

Okamoto, N. and Nakazawa, M. (1979). "Finite element incremental contact analysis with various frictional conditions", *Int. J. Num. Meth. Engrg.* **14**, 337-357.

Plesha, M. and Belytschko, T. (1985). "On the modeling of contact problems with dilation", *Studies in Appl. Mech.-Mech. of Mat. Interfaces*, Series 11, Ed. A.P.S Selvadurai and G.Z. Boyiadjis, 63-77.

Rabbat, B. G. and Russell, H. G. (1988). "Friction coefficient of steel on concrete", *J. Struct. Engrg.* **111** (3), *ASCE*, 505-515.

Sachdeva, T.D. and Ramakrishnan, C. V. (1981). "A finite element solution for the two-dimensional elastic contact problems with friction", *Int. J. Num. Meth. Engrg.* **17**, 1257-1271.

Torstenfelt, Bo R. (1983). "Contact problems with friction in general purpose finite element computer programs", *Comput. Struct.* **16** (1-4), 487-493.

Yamaguchi, E. and Chen, W. F. (1990). "Cracking model for finite element analysis of concrete materials". *J. Mech. Engrg, ASCE,* **116** (6), 1242-1260.
Zienkiewicz, O. C. (1977). *The Finite element method.* McGraw-Hill, 3rd ed., New York.

Notation

$\underset{\sim}{d}$	relative interface displacement vector of a candidate pair of nodes
$\underset{\sim}{\Delta d}$	increments of vector $\underset{\sim}{d}$
E_c	Young's modulus of concrete
E_s	Young's modulus of steel
$\underset{\sim}{f}$	interface nodal force vector
f_c'	ultimate compressive strength of concrete
f_y	yield strength of steel
F	criteria function at interface
h	interface material modulus
k	interface elementary stiffness
K_T	tangential stiffness matrix of global system
$\underset{\sim}{n}$	outward normal boundary vector
$\underset{\sim}{R}$	residual vector of global system
$[R]$	transformation matrix
$\underset{\sim}{u}$	vector of displacements in local system
$\underset{\sim}{U}$	displacement vector of global system
$\underset{\sim}{x}$	coordinate vector of a candidate pair of nodes

superscripts

c	refers to concrete
s	refers to steel
*	refers to virtual

symbols

α	index referring to configurations
β	index referring to concrete and steel
ε	strain vector at the interface
$\underset{\sim}{\gamma}$	interface displacement vector
$[\kappa]$	stiffness matrix of interface
μ	friction coefficient
$d\lambda$	scalar
$\underset{\sim}{\lambda}^*$	virtual displacement vector at the interface
Φ	interface slip potential function
$\underset{\sim}{\sigma}$	stress tensor at the interface
σ_t	interface shear resistance
σ_w	interface degradation constant
ω	degradation of interface shear resistance

subscripts

c	refers to concrete

i, j, k, l, m	indices referring to coordinate axes
n, t	refers to normal and tangential directions, respectively
eq	refers to equivalent value
I	refers to interface
s	refers to steel